Field-Swept Magnetic Particle Spectroscopy: A Single-Harmonic Method for Simultaneous Determination of Magnetic Nanoparticle Types and Quantities

Yanjun Liu[1,2,3,4,5], Xin Feng[4,5,6], Haoran Zhang[1,2,3,4,5], Sijia Liu[4,5,7], Guanghui Li[1,2,3], Yu An[1,2,3,4,5], Hui Hui[4,5,6], and Jie Tian[1,2,3,4,5,7], *Fellow, IEEE*

[1]School of Engineering Medicine, Beihang University, Beijing 100191, China
[2]School of Biological Science and Medical Engineering, Beihang University, Beijing 100191, China
[3]Key Laboratory of Big Data-Based Precision Medicine (Beihang University), Ministry of Industry and Information Technology, Beijing 100191, China
[4]CAS Key Laboratory of Molecular Imaging, Institute of Automation, Chinese Academy of Sciences, Beijing 100190, China
[5]Beijing Key Laboratory of Molecular Imaging, Beijing 100190, China
[6]School of Artificial Intelligence, University of Chinese Academy of Sciences, Beijing 100080, China
[7]School of Computer Science and Engineering, Southeast University, Nanjing 210096, China

Magnetic particle spectroscopy (MPS) allows for highly sensitive and real-time characterization of magnetic nanoparticles (MNPs). When combined with surface-modified MNPs that can specifically bind to biomarkers, MPS can serve as a quantitative biosensing platform and has shown enormous potential in point-of-care diagnosis. To improve diagnostic efficiency and accuracy, the simultaneous detection of multiple biomarkers has been studied in MPS, which requires the simultaneous determination of the type and quantity of MNPs. Current methods generally rely on the higher order harmonics (e.g., third to fifth harmonic ratio) of the MNPs' magnetic responses to the excitation fields, but facing challenges at low concentrations or with small-sized MNPs that are difficult to generate sufficient harmonics. In this article, we propose a single-harmonic method for simultaneous determination of MNP types and quantities, named field-swept MPS (FS-MPS). An adjustable static magnetic field perpendicular to the alternating magnetic field is introduced and MNPs' field-dependent response is registered from the static field direction. By comparing the simulation results of serval system configurations and the field-swept spectra of different harmonics, we found that the second harmonic component of the MNP signal combines good specificity and robustness with no direct feed-through interference issues. We built the first FS-MPS device and carried out the experiments of binary MNP mixtures to verify the effectiveness of the proposed method. Our experimental results showed that the proposed method has up to 90% accuracy for the simultaneous determination of two types of MNPs with a maximum concentration ratio of 9:1. The proposed method can in principle determine more types of MNPs simultaneously, providing an effective tool for the detection of multiple biomolecular markers.

***Index Terms*— Magnetic nanoparticles (MNPs), magnetic particle spectroscopy (MPS), multiplexed biosensing, point-of-care diagnosis.**

I. Introduction

THE unique superparamagnetic properties of magnetic nanoparticles (MNPs) combined with appropriate surface functionalization enable them to be used in a wide range of biomedical scenarios, such as heat sources for hyperthermia, carriers for targeted drug delivery, contrast agents in magnetic resonance imaging, and tracers in magnetic particle imaging (MPI) [1], [2], [3], [4], [5], [6], [7], [8]. Since the performance of MNPs in their intended applications is highly dependent on the magnetic properties and surface modifications of the MNPs, a variety of different methods and techniques are available today for characterizing MNPs [9], [10], [11], [12].

Magnetic particle spectroscopy (MPS) is a relatively young technique derived from MPI that allows quantitative detection of MNP concentration in biological tissues or in vitro samples by measuring the nonlinear magnetization response of MNPs [13], [14], as well as highly sensitive and immediate characterization of the magnetic properties and hydrodynamic parameters (e.g., viscosity, temperature, and hydrodynamic diameter) of MNPs [15], [16]. The MPS technique was initially used for tracer selection and performance optimization of MPI, but today, it has developed into an important research platform in the field of biomarker detection and magnetic immunoassay by virtue of its ease of use, rapidity, high sensitivity, and low cost [17], [18], [19], [20], [21], [22].

Recently, several MPS research groups have made landmark progress in characterizing single MNPs (MNPs with the same magnetic properties) for applications [23], [24], [25], [26], [27], while multi-particle (MNPs with different magnetic properties) characterization techniques are also rapidly developing [28], [29], [30], [31]. It is conceivable that it would be very useful for different MNPs to be quantitatively identified simultaneously in a biologically meaningful sample. Just as enzyme linked immunosorbent assay uses probes with different optical properties to label multiple biomedical targets, the specific magnetic properties of MNPs can be

Manuscript received 27 January 2023; revised 19 March 2023 and 9 May 2023; accepted 16 May 2023. Date of publication 25 May 2023; date of current version 28 June 2023. Corresponding authors: X. Feng; H. Hui; and J. Tian (e-mail: xin.feng@ia.ac.cn; hui.hui@ia.ac.cn; tian@ieee.org).

Color versions of one or more figures in this article are available at https://doi.org/10.1109/TMAG.2023.3279930.

Digital Object Identifier 10.1109/TMAG.2023.3279930

used as "colors" in the MPS assay. There are many potential applications including magnetic fingerprints, in vitro analysis of MNPs in cell culture, monitoring of MNP synthesis processes, and multi-color MPI [32], [33], [34].

Previous MPS used the ratio of harmonics to characterize MNP properties, while relying on as many higher order harmonics as possible when quantifying multi-particle mixtures [28], [29]. However, the absolute amplitude of each harmonic decreases with increasing order, so that higher harmonics are susceptible to background noise when the concentration of MNPs is low. In addition, the magnetization response of small-sized MNPs is mainly linear, so they may not have higher harmonics. There are some improved methods that utilize relatively few harmonics, such as an amplitude sweep method at very low frequencies (200 Hz) for estimating the core size distribution and a frequency sweep method at mixed frequency excitation for identifying different MNPs [31], [32], [33], [34], [35]. However, the effectiveness of these methods is limited to specific excitation modes and frequencies, so there are still limitations in terms of generalizability of applications. Previous work has suggested that further improvements can be achieved by varying the frequency and amplitude of the excitation magnetic field [29], [30], but to the best of our knowledge, there are not enough scheme design and experimental studies to date.

In this article, we present a field-swept MPS (FS-MPS) by using an alternating magnetic field (ac field) with fixed amplitude and a static magnetic field (dc field) with adjustable amplitude along the orthogonal direction. The proposed method essentially introduces a new parameter space by measuring the harmonic response curves of MNPs to the dc field. We mathematically formulate the multi-particle quantification task as a Fredholm integral equation and then evaluate the condition number of the equation for different excitation modes. The first desktop FS-MPS device was developed and performed for the quantitative detection of binary MNP mixtures. The experimental results demonstrate the detection accuracy of the proposed method up to 90% for binary MNP mixtures with a maximum concentration ratio of 9:1. The proposed method enables the identification of various MNPs using the field-swept response curve of a single harmonic without relying on multiple higher order harmonics, which is significant in the absence of sufficient higher order harmonics, such as small amplitude excitation and small size or low concentration of particle samples.

II. Theory and Methods

A. Theoretical Formulas

The magnetization of MNPs sample depends on the applied magnetic field H. In the absence of an applied magnetic field, the magnetic moments of all MNPs in the sample are oriented randomly, which leads to zero magnetization. Increasing the strength of the H leads to an increasing number of MNPs aligned along the external magnetic field, which in turn leads to an increase in the magnetization M of the sample. When interparticle interactions are not considered, the total magnetization of MNPs with different properties in the sample is

$$M_{\text{Total}}(H) = \sum_{i=1}^{I} M_i(H), \quad I \in \mathbb{N} \tag{1}$$

where M_i is the magnetization of the ith kind of MNPs in the sample. In MPS, both the applied magnetic field and the receive coil sensitivity are generally homogeneous. When the sample volume is constant, according to Faraday's law, the induced voltage of the total magnetization can be expressed as the sum of the slew rates of all magnetic moments in the sample

$$u[H(t)] = -\mu_0 \sum_{i=1}^{i} N_i \frac{d\bar{m}_i(H)}{dH} \frac{dH(t)}{dt} \tag{2}$$

where N_i is the number of the ith MNP in the sample, and $\bar{m}_i$ is the mean magnetic moment of the ith MNP. Then, the Fourier transform of both ends of (2) is as follows:

$$\hat{u}_k(H) = \sum_{i=1}^{I} N_i A_k(\bar{m}_i, H), \quad k \in \mathbb{N} \tag{3}$$

where $\hat{u}_k(H)$ is the kth harmonic component of the total voltage signal, and $A_k(\bar{m}_i, H)$ is the contribution weight of the ith MNP to the kth harmonic amplitude. Equation (3) is a discrete Fredholm integral equation, where N_i is the unknown to be solved and $\hat{u}_k$ is the measured data. In general, the number of equations should be no less than the number of unknowns. The previous method uses harmonic components of multiple frequencies to construct equations, while ours expands the number of equations of a specified frequency harmonic by changing the external field amplitude, which is called FS-MPS. Take the second harmonic as an example

$$\hat{u}_2(H_j) = \sum_{i=1}^{I} N_i A_2(\bar{m}_i, H_j), \quad j = 1, 2, \ldots, J, \quad J \in \mathbb{N}. \tag{4}$$

The matrix form of the above equation is

$$\begin{bmatrix} \hat{u}_2(H_1) \\ \vdots \\ \hat{u}_2(H_J) \end{bmatrix} = \begin{bmatrix} A_2(\bar{m}_1, H_1) & \cdots & A_2(\bar{m}_1, H_1) \\ \vdots & \ddots & \vdots \\ A_2(\bar{m}_1, H_J) & \cdots & A_2(\bar{m}_1, H_J) \end{bmatrix} \begin{bmatrix} N_1 \\ \vdots \\ N_I \end{bmatrix} \tag{5}$$

or

$$\mathbf{u} = \mathbf{A}\mathbf{N}. \tag{6}$$

The element of the coefficient matrix $\mathbf{A}$ represents the kth harmonic amplitude of the ith MNP under the jth applied field, which can be measured in advance using a sample of the same MNP per unit concentration. In this case, N_i is the ratio to the unit concentration of the ith MNP. The coefficient matrix $\mathbf{A}$ is generally overdetermined, because the number of fields in the measurement vector $\mathbf{u}$ is more than the number of different kinds of MNPs, that is, $J > I$. There are many mathematical methods for solving linear equations. The singular value decomposition (SVD) method is adopted here, and the SVD of matrix $\mathbf{A}$ is as follows:

$$\mathbf{A} = \mathbf{U}^* \mathbf{\Sigma} \mathbf{V}^{*\,\mathrm{T}} \tag{7}$$

with

$$\mathbf{\Sigma} = \mathrm{diag}\left[\sigma_1, \sigma_2, \ldots, \sigma_{p-1}, \sigma_p\right] \tag{8}$$

where $\mathbf{U}^*$ and $\mathbf{V}^*$ are the orthogonal matrices of $J \times J$ and $I \times I$, respectively, $\mathbf{\Sigma}$ is a diagonal matrix of $J \times I$, σ_p is the pth singular value of $\mathbf{A}$, and P is the rank of $\mathbf{A}$. The pseudo-inverse matrix $\mathbf{A}^{-1}$ of $\mathbf{A}$ is constructed by SVD, and the solution of (6) is

$$\hat{\mathbf{N}} = \mathbf{A}^{-1}\mathbf{u} = \mathbf{V}^*\mathbf{\Sigma}^{-1}\mathbf{U}^{*\mathrm{T}}\mathbf{u} \tag{9}$$

with

$$\mathbf{\Sigma}^{-1} = \mathrm{diag}\left[\frac{1}{\sigma_1}, \frac{1}{\sigma_2}, \ldots, \frac{1}{\sigma_P}\right] \tag{10}$$

where $\mathbf{\Sigma}^{-1}$ is a diagonal matrix of $I \times J$. From the above equations, $1/\sigma_P$ is extra sensitive to measurement errors in $\mathbf{u}$ when σ_P is very small. The alternative solution to improve the robustness is to discard the small singular values using truncated SVD (TSVD), but this is a lossy operation that will deviate from the true value if mishandled. Therefore, we expect the original coefficient matrix to have a more concentrated distribution of singular values. No singular values are discarded in this study, and a relatively robust coil configuration is determined by simulation analysis in Section II-B.

B. Comparison of Field Sweep Plans

As described in Section II-A, the quantitative detection of multi-particle mixtures can be mathematized as a task of solving a linear system of equations. Therefore, the detection accuracy depends on the performance of the coefficient matrix $\mathbf{A}$. Several metrics can be used to evaluate the performance of the coefficient matrix, such as the rank and condition number of the matrix. The rank of the coefficient matrix indicates the number of independent equations and preferably should be no less than the number of unknowns, which can be achieved by FS-MPS. The condition number indicates the ill-conditioning of the system of equations, and a larger condition number means that the system of equations is more sensitive to noise. Since the coefficient matrix essentially originates from the field-dependent curves of specific harmonics of different MNPs, the optimal design of the applied field in FS-MPS is crucial to enhance the performance of the coefficient matrix and the effectiveness of the proposed method.

In order to analyze the performance of different field sweep plans in distinguishing different MNPs, we used Langevin function to simulate the nonlinear response of MNPs. The saturation magnetization of the particles is 0.6 T/μ_0, and the absolute temperature is 298 K. The magnetic field setting of the specific plan was described as follows.

Previous MPS generally used an ac field H_{ac} to excite the MNPs alone. In this study, we considered the bias field effect by adding a dc field H_{dc} parallel or perpendicular to the ac field [27], [36], which will lead to more options. Defining the received magnetization direction as the z-direction, the four magnetic field sweep plans were as follows:

$$\begin{aligned}
&\text{Plan A}: \quad \boldsymbol{H}_j(t) = H_{\mathrm{ac}}^j(t)\boldsymbol{z}\\
&\text{Plan B}: \quad \boldsymbol{H}_j(t) = \left[H_{\mathrm{dc}}^j + H_{\mathrm{ac}}(t)\right]\boldsymbol{z}\\
&\text{Plan C}: \quad \boldsymbol{H}_j(t) = H_{\mathrm{dc}}^j\boldsymbol{x} + H_{\mathrm{ac}}(t)\boldsymbol{z}\\
&\text{Plan D}: \quad \boldsymbol{H}_j(t) = H_{\mathrm{dc}}^j\boldsymbol{z} + H_{\mathrm{ac}}(t)\boldsymbol{x}.
\end{aligned} \tag{11}$$

The coil configurations of the four magnetic field sweep plans were shown in Fig. 1(a). Plan A used a conventional MPS configuration with a compensation coil reversed to the receive coil to counteract the direct feedthrough from the ac field [26]. Plan B added a dc field in the same direction as the ac field, which causes the MNPs to produce odd and even harmonics simultaneously [27]. Therefore, for Plan B, two alternative subschemas are analyzed here including the use of the third harmonic (Plan B.1) or the second harmonic (Plan B.2), as shown in Fig. 1(b). Plan C added a dc field perpendicular to the ac field based on Plan A. Plan D is a relatively novel coil configuration that allows the receive coil to pick up the magnetization component in the direction of the dc field. A significant advantage of Plan D is the avoidance of direct feed-through issues of the ac field, which is expected to improve the detection limit of MNPs [37].

To determine the optimized coil configuration, we compared the performance of the coefficient matrixfor different magnetic field configurations by simulations. The harmonic spectra of MNPs with three different core sizes (20, 25, and 30 nm) in different coil configurations were simulated, as shown in Fig. 1(b), where the ac field amplitude was set to 10 mT and the dc field amplitude was set to 3 mT. Different excitation modes result in different harmonic properties in the received signal. The simulation results showed that there are only odd harmonics in Plans A and C, and only even harmonics in Plan D, while Plan B has both odd and even harmonics. Since the direct feedthrough may potentially affect the reliability of the fundamental frequency component, we choose either the second or third harmonic.

Each column of the coefficient matrix of the different plans was plotted separately, as shown in Fig. 1(c). Here, the swept field was increased from 0 to 10 mT. To demonstrate the nonlinear correlation between different columns, the values of each column were normalized to a range from 0 to 1. At this moment, the differences between the different MNPs can be clearly seen, and the larger differences imply that they are more easily distinguished simultaneously.

The condition numbers of the different coefficient matrices were calculated, as shown in Fig. 2, which directly quantifies the performance of the coefficient matrices, and the smaller condition numbers indicate that the coefficient matrices of the corresponding plans are better. Fig. 2 demonstrates that Plans A, B.1, and D have similar good performance at large fields, while Plan D performs better at low fields. Plan C is relatively smooth but has a higher condition number level. Plan B.2 is sensitive to the swept field range and is only effective at high fields. The performance of the condition number can be explained by Fig. 1(c). The more similar magnetic response characteristics of different particles lead to higher linear correlation between the column profiles of the

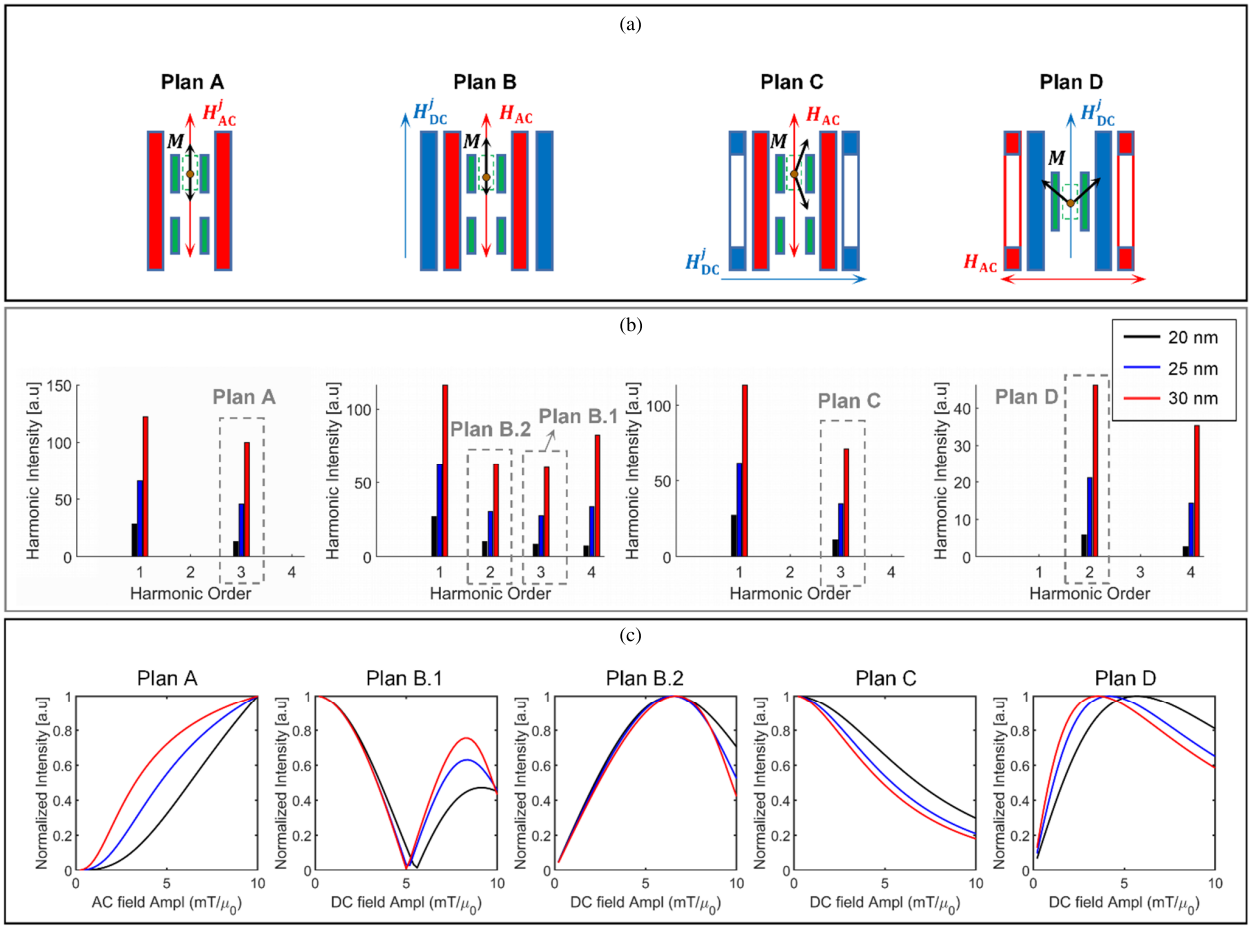

Fig. 1. Simulation comparison of different swept field plans. (a) Coil configurations of different plans. Red represented the ac field coil, blue represented the dc field coil, and green represented the receive and compensation coil. The receive coil in Plan D was orthogonal to the ac field coil, avoiding the direct feed-through issue, so the compensation coil was not needed. The red arrow indicates the direction of the ac field, the blue arrow indicates the direction of the dc field, and the black arrow indicates the direction of magnetization. (b) Harmonic spectra of the MNP signals in different plans. To avoid the effect of direct feedthrough, lower order harmonics (second or third harmonic) other than fundamental frequency were selected for analysis. (c) Coefficient matrices under different plans, the values of each column were normalized to 0–1.

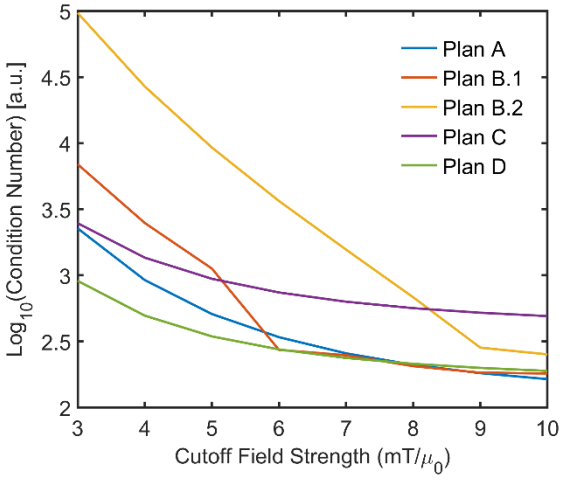

Fig. 2. Condition number of coefficient matrix for different plans. The cutoff field strength indicates the upper limit of the swept field range.

coefficient matrix, which makes the solution of the equation more sensitive to small noise. As shown in Fig. 1(c), the profiles of the three particles in the low-field region of Plans B.1 and B.2 almost overlap, while Plan D in comparison remains more different throughout the dc field range, which is consistent with the results in Fig. 2. After a comprehensive analysis, we choose Plan D to develop the FS-MPS device, an important reason being that Plan D has good coefficient matrix performance while greatly avoiding the effects of direct feed-through interference.

C. MNP Samples Preparation

Two commercially available MNPs were studied, including Synomag[1]-D with hydrodynamic diameters of 70 and 50 nm (Micromod GmbH, Germany). The Synomag-70 MNP used had an amino group on its surface and the stock solution sample had an iron concentration of 6 mg/mL. The Synomag-50 MNP used had an unmodified dextran surface and the stock solution sample had an iron concentration of 10 mg/mL. Transmission electron microscope (TEM) images of two MNPs were shown in Fig. 3. Two MNPs in different concentrations were mixed in a 200 μL vial for subsequent measurements.

[1]Registered trademark.

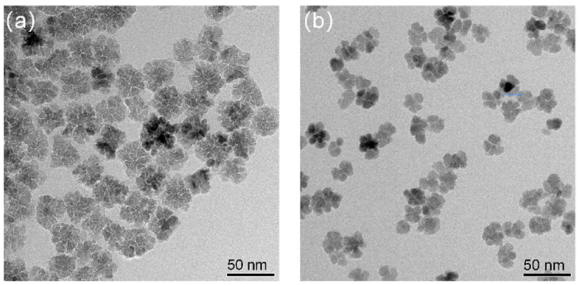

Fig. 3. TEM images of two MNP samples. (a) Synomag-70. (b) Synomag-50. The iron cores of the two particles have different size distributions. Synomag-70 particles are estimated to be in the range of 25–30 nm and Synomag-50 particles are estimated to be in the range of 18–24 nm.

III. Experimental Results

A. Field-Swept Magnetic Particle Spectrometer

A tabletop spectrometer for FS-MPS was developed in this work, providing a highly sensitive and flexible experimental platform. Significant modifications over conventional MPS devices included the addition of a dc field coil with adjustable amplitude along the induction direction of the receive coil and the fact that the direction of the ac field was orthogonal to the direction of the receive coil. The proposed FS-MPS device was shown in Fig. 4. The ac field was generated by a Helmholtz coil made by winding 56 turns of Litz wire with 350 × 0.1 mm strands. The optimized inductance was 260 μH allowed the coil to generate a cosine alternating field of 10 mT/μ_0 in the frequency of 0–5 kHz. The dc field was generated by a 22-turn solenoid coil with a resistance of 48 mΩ and adjustable amplitude in the range of 0–10 mT/μ_0. The receive coil was a 240-turn solenoid wound with 0.2 mm lacquered copper wire with a diameter of 10 mm, aligned with the direction of the dc field. A data acquisition card (DAQ) was used to generate ac and dc signals fed to power amplifiers (AE 7548 and AE 7224, AE Techron, USA). Two current probes (DS50UB-10V, Danisense, DNK) were used to monitor the current in the ac and dc coils and feed it back to the DAQ (NI-USB 6356, National Instruments Corporation, USA). The induced voltage signals from the receive coil were transmitted to the low-noise preamplifier (LNA) (SR560, Stanford Research System, USA) and finally to the DAQ for recording. The sampling rate was 1 MS/s The even harmonics of the received signal were extracted and analyzed by digital phase-sensitive detection (DPSD).

Prior to the MNP mixture experiments, the MNPs used were pre-characterized using the developed spectrometer. Fig. 5 showed the typical voltage signals of the Synomag-70 and Synomag-50 samples with an iron concentration of 1 mg/mL, and the simultaneously monitored magnetic field waveforms, where the ac field frequency was 2.5 kHz and the amplitude was set to 10 mT and the dc field amplitude was set to 3 mT.

Unlike the conventional MPS signal [18], the signal detected here is a magnetization component orthogonal to the ac field, shaped like a sawtooth wave, and the period of the signal is half the period of the ac field. The signal intensity of Synomag-70 is about 1.85 times higher than that of Synomag-50, which is related to the larger equivalent core diameter. Since the magnetization component in the dc field direction reaches its

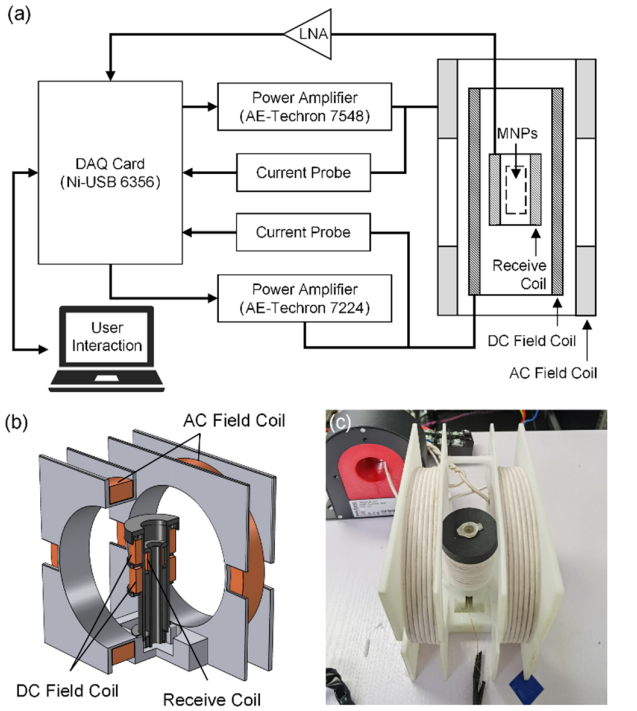

Fig. 4. Tabletop FS-MPS device. (a) Schematic of the system composition showing all necessary modules, such as transmit/receive coils, ac/dc power amplifiers, LNA, current probes, DAQ card, and user interaction module. (b) Three-dimensional structure diagram of the transmit/receive coils. (c) Photograph of the coils.

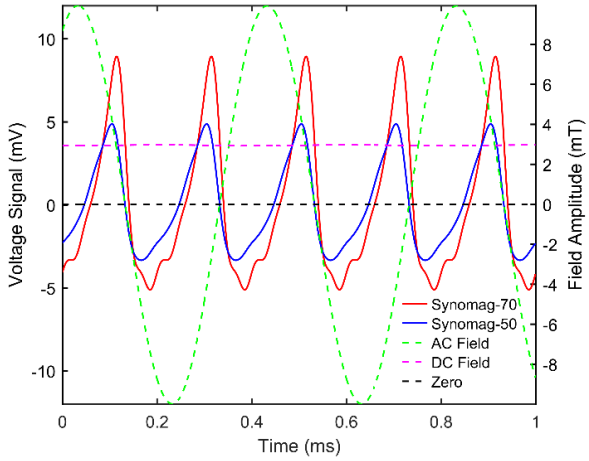

Fig. 5. Induced voltage signal of MNPs along the dc field direction and applied fields. The intensity of the particle signal was amplified by a factor of 5. The ac field amplitude was set at 10 mT and the frequency was 2.5 kHz. The amplitude of the dc field was 3 mT. The iron concentration of the two samples was 1 mg/mL.

extremes when the ac field is zero, the trans-zero point of the voltage signal should intersect the trans-zero point of the ac field according to Faraday's law of electromagnetic induction. However, the signal of Synomag-70 has a small phase lag, which may be due to the relaxation mechanism of large-size MNPs, which requires further frequency-dependent studies.

The signal data in Fig. 5 can be transformed into M–H dynamic hysteresis loops and Fourier spectra for more intuitive characterization of the particles, as shown in Fig. 6. According to Faraday's law of electromagnetic induction, the change

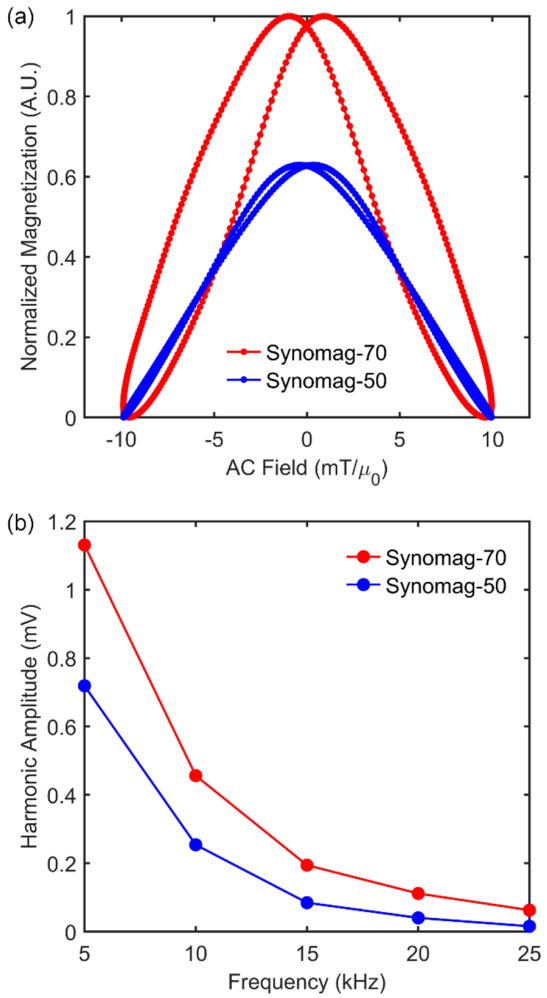

Fig. 6. (a) M–H dynamic hysteresis loop. (b) Fourier spectrum. The ac field amplitude was set at 10 mT and the frequency was 2.5 kHz. The amplitude of the dc field was 3 mT. The iron concentration of the two samples was 1 mg/mL.

of magnetization with ac field can be qualitatively derived from the integration of the induced voltage signal over time. Fig. 6(a) shows the dynamic hysteresis loops during one excitation period. Unlike the conventional hysteresis loop, the perpendicular dc field-induced magnetization component exhibits a double-peaked curve, as shown in Fig. 6(a). The peak-to-peak distance of the Synomag-70 MNP curve is significantly larger than that of Synomag-50, which is consistent with the signal phase lag phenomenon in Fig. 5. A potential trigger is due to the fact that Synomag-70 MNP has a larger iron core thus leading to more pronounced relaxation effects, which requires further frequency-dependent studies.

Fig. 6(b) showed the frequency spectra of the voltage signals obtained by Fourier transform, which are mainly the even harmonic. Since the ac field frequency is 2.5 kHz, the observed frequencies are even multiples of 2.5 kHz, e.g., 5 and 10 kHz correspond to the second and fourth harmonics of the MNP, respectively. As expected, the harmonic amplitude decays rapidly with increasing order. From the second harmonic to the tenth harmonic, the signal-to-noise ratio (SNR) of Synomag-70 is attenuated from 44 to 19 dB, while Synomag-50's SNR is attenuated from 40 to 7 dB. The ratios of

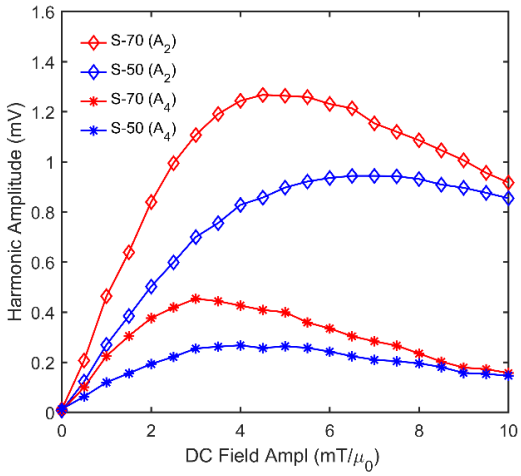

Fig. 7. Prior measurements of reference samples. The FS-MPS data of two MNP samples per unit iron concentration form the coefficient matrix. Here, A_2 and A_4 denote the second and fourth harmonic amplitudes, respectively.

the fourth and second harmonics (A_4/A_2) were calculated to be 0.4036 and 0.3533 for Synomag-70 and Synomag-50, respectively, which indicates the greater ability of Synomag-70 to generate higher harmonics. In a comprehensive analysis, Synomag-70 with larger size has stronger nonlinear response and larger effective magnetic moment than the Synomag-50 for the given excitation parameters in this study.

B. Field-Swept Magnetic Particle Spectrum

The two MNPs were diluted to an iron concentration of 1 mg/mL and each was put into a 200 μL vial for measurement. The amplitude of the perpendicular static field changes from 0 to 10 mT with the step size of 0.5 mT. The harmonic amplitude of the measured signal was extracted by DPSD and plotted as curves shown in Fig. 7. The field-swept spectrum curves of the two MNPs with the same iron concentration are significantly different. Although both have an obvious maximum value, the signal intensity of Synomag-70 (S-70) is higher than that of Synomag-50 (S-50), and the dc field amplitude corresponding to the maximum value is smaller than that of S-50. This phenomenon is consistent with the numerical simulation results (see Fig. 1) because S-70 has a larger equivalent core size than S-50. As expected, the second harmonic amplitude is overall more than 3 times higher than the fourth harmonic, with a higher SNR, which is very important for quantitative estimation. In addition, (4) has shown that the effect of the MNP quantity on the harmonic amplitude is linear and does not change its shape. Therefore, we can construct the coefficient matrix using the second harmonic data in Fig. 7.

The sensitivity of the current FS-MPS device was pre-evaluated prior to the preparation of the mixture samples. Using Synomag-70 MNP as an example, the concentration of the sample was kept constant, and then, the sample volume in the tube was reduced sequentially until the signal intensity converged to the background noise level. Repeated test results showed that the sample with an iron content of 3 μg could still be effectively detected, as shown in Fig. 8. It can be seen that under iron content of 3 μg, the mean signal strength at 5 mT is about 9.3 times (66.58/7.15 μV) that of noise.

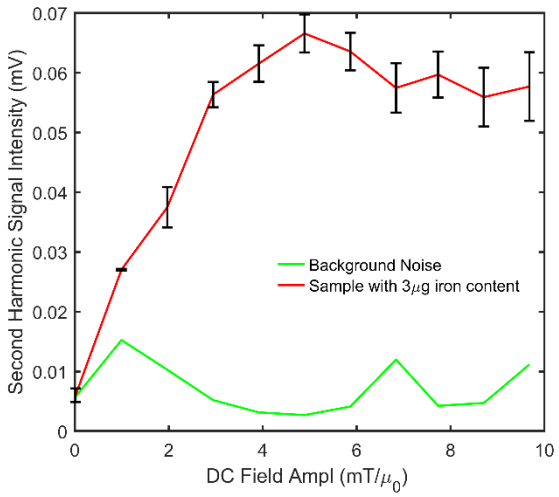

Fig. 8. First evaluation of the detection sensitivity of the FS-MPS system. The MNPs sample with 3 μg iron was effectively detected.

C. Simultaneous Quantification of MNP Mixtures

By gradually increasing the amplitude of the dc field, we can obtain the number of equations far more than the type of MNPs but lead to an increase in the measurement time. The average measurement time for each field amplitude is 1 s, and changing the amplitude J times means consuming at least J seconds. To balance the detection accuracy and time, we compared the quantitative detection results of mixtures with different numbers of field-swept points, as shown in Fig. 9.

The dc field amplitudes used start at 1 mT and increased in steps of 1 mT. For example, if the number of field-swept points was 3, the measured data of dc fields of 1, 2, and 3 mT were used. The number of field-swept points determines the number of rows of the coefficient matrix, i.e., the number of equations. Fig. 9(a) showed the condition number of the coefficient matrix with different numbers of field swept points, which decreases and flattens out as the number of field-swept points used increases. The condition number of the coefficient matrix using ten field-swept points is 15.13, and there is still a downward trend, but this is no longer significant. Fig. 9(b) showed the quantitative estimation results using data with different number of field-swept points. When more than eight points were used, the estimated values tended to be close to the true values. The results indicate that for binary mixtures, more field-swept data may be redundant. The MNP concentration in the mixed sample can be accurately estimated using ten field-swept points. At this moment, the whole detection process took about 10 s.

To verify the effectiveness of the proposed method in the simultaneous detection of multi-particle mixtures, a series of mixtures of Synomag-70 and Synomag-50 with different concentration ratios were prepared. The volume of both MNP samples before mixing was 100 μL. The concentration of Synomag-70 decreased from 0.5 mg/mL in sample #1 to 0.1 mg/mL in sample #7, and conversely, Synomag-50 increased from 0.5 to 0.9 mg/mL. The concentration of each MNP was estimated using ten field-swept point data, and the experimental results were shown in Fig. 10.

Fig. 10(a) showed the quantitative composition of the two MNP mixtures estimated using the FS-MPS technique. The estimation error increases when the content of the two MNPs differs significantly. Fig. 10(b) showed the analysis of the relative error between the estimated and true values, with the maximum error within 10%. The detailed quantification results and mean relative errors (MREs) were shown in Table I.

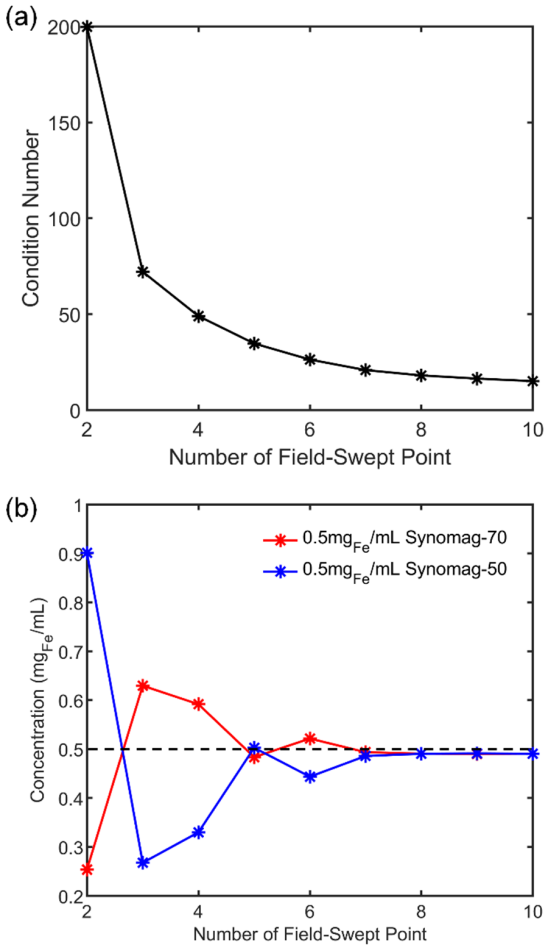

Fig. 9. Influence of the number of field-swept points on inversion estimation results. (a) Condition number of the coefficient matrix with different number of field-swept points. (b) Quantitative estimates of mixture samples using coefficient matrices with different numbers of field-swept points. The concentration of Synomag-70 and Synomag-50 was 0.5 mg/mL and the volume ratio was 1:1.

TABLE I
QUANTIFICATION RESULTS FOR THE BINARY MIXTURE

Sample ID	Synomag-70		Synomag-50	
	Real	Estimated	Real	Estimated
	Unit: mg$_{Fe}$/mL		Unit: mg$_{Fe}$/mL	
#1	0.501	0.491	0.500	0.490
#2	0.399	0.402	0.600	0.579
#3	0.324	0.319	0.675	0.662
#4	0.249	0.263	0.750	0.733
#5	0.210	0.217	0.790	0.753
#6	0.160	0.171	0.840	0.805
#7	0.100	0.109	0.900	0.839
MREs	**4.26%**		**3.60%**	

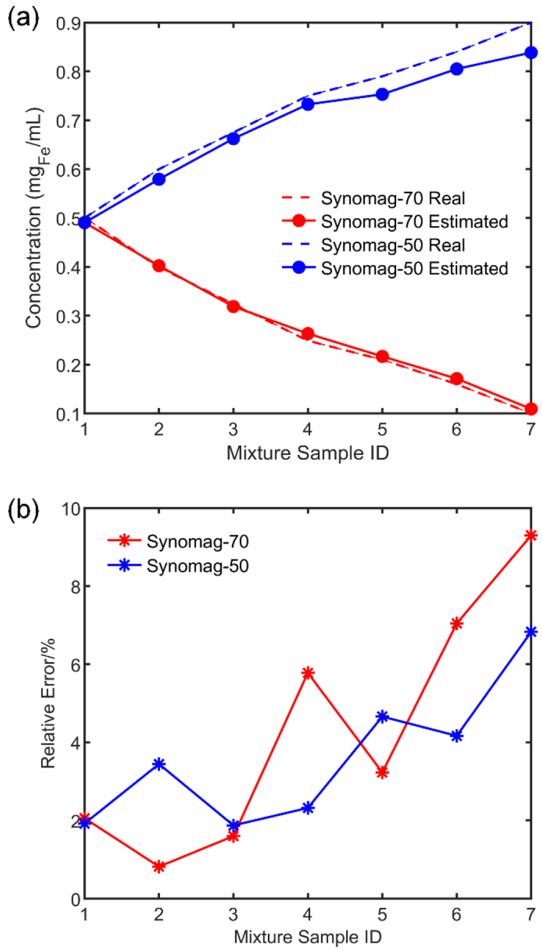

Fig. 10. Experimental results of mixture samples with different concentration ratios. (a) Simultaneous quantification of the concentration of the two MNP samples. (b) Relative error between estimated value and true value.

IV. Discussion and Conclusion

In this study, the concept of FS-MPS was proposed to simultaneously determine the types and quantities of multiple MNPs. Various field-swept plans are compared by simulations to determine the optimal coil configuration for the FS-MPS device. By applying a perpendicular dc field, MNPs are induced to produce second harmonics that are sensitive to the MNP properties. The second harmonic used here comes from the magnetization component in the direction of the dc field, which is geometrically orthogonal to the ac field, achieving separation from direct feed-through interference. By measuring the second harmonics at different dc field amplitudes, a linear system of equations is constructed to quantitatively decompose the signal of a mixture containing two MNPs. A series of experimental results with different mixing ratios show that the quantification error is positively correlated with the difference of MNP concentrations in the mixtures. The quantification accuracy is above 90% when the concentration difference between the two MNPs is less than 9:1.

Existing studies for using multiple fields to excite MNPs have been summarized in [17] and [18], including a combination of ac field and dc field with a small amplitude [19], or multiple ac fields with different amplitudes but no dc field [28]. Here, we introduce FS-MPS, a novel method that uses a fixed ac field combined with an adjustable dc field along the orthogonal direction. FS-MPS essentially introduces a new parameter space by measuring the harmonic response spectra of MNPs to dc fields. The identification of various MNPs can be achieved using the response spectra of a single harmonic instead of relying on multiple high-order harmonics, which is particularly useful in scenarios with few high-order harmonics, such as small-amplitude excitation and small-size or low-concentration particle samples.

The swept field in this study ranges from 1 to 10 mT, which is sufficient for accurate quantification of the two MNP mixtures here, and the whole measurement process is completed in about 10 s. Simultaneous quantification of more than two MNP mixtures is to be expected because the number of equations is much larger than the number of unknowns.

Noted that under iron content of 3 μg, the mean signal strength at 5 mT is about 9.3 times the mean noise (66.58/7.15 μV), so the estimated detection limit of the current system is about 0.32 μg iron, which implies a minimum iron concentration of approximately 1.6 μg/mL (28.7 nmol/mL) for a 200 μL volume of sample theoretically. The detection sensitivity of FS-MPS device can be further optimized by increasing the frequency and amplitude of the ac field. Commercial MNPs (Perimag, Micromod GmbH, Germany) with 150 μg iron were detected in a multi-spectral MPS (1 kHz, 25 mT) reported in 2019 [29]. Functionalized MNPs with 2.5 μg iron were detected in a critical offset MPS (20 kHz, 50 mT) reported in 2022 [27]. We would like to emphasize that the current detection sensitivity of hardware system can be further improved by increasing the excitation frequency and amplitude, which does not represent the detection limit of the proposed single-harmonic method. Since the sensitivity is also related to the amplification factor of the receive chain as well as to the background noise level, a more meaningful investigation would be to compare the detection sensitivity of different harmonics in the same system. The study reported that the detection sensitivity of the second harmonic is 10 times higher than that of the fifth harmonic in the same system [26], which further confirms the advantage of the single-harmonic method proposed in this article over multiple higher harmonic methods. Since FS-MPS was first proposed for the detection of multi-particle mixtures, we conducted a typical binary mixture experiment to verify the effectiveness of the method. More practical experiments will be conducted in the next step.

In addition, we found that the extreme point of the curve of the second harmonic with dc field is highly specific to the MNP, and the stronger the MNP magnetism, the smaller the dc field strength of the extreme point, which is confirmed by simulation and experiment. We believe that this parameter is very useful for the instantaneous differentiation of different MNPs (or MNPs with different viscosities, temperatures, and binding states), which will be further investigated in the future. In summary, the proposed method is a rapid, sensitive, and robust tool for the simultaneous quantification of MNP mixtures and has promising applications for multi-parameter measurements based on MNPs and quantitative detection of biomarkers.

ACKNOWLEDGMENT

This work was supported in part by the National Key Research and Development Program of China under Grant 2017YFA0700401; in part by the National Natural Science Foundation of China under Grant 62027901, Grant 81827808, Grant 81930053, and Grant 81227901; in part by the Beijing Natural Science Foundation under Grant JQ22023 and Grant 7232346; in part by the Chinese Academy of Sciences (CAS) Youth Innovation Promotion Association under Grant Y2022055; and in part by the Guangdong Key Research and Development Program of China under Grant 2021B0101420005.

The authors thank Dr. Zhong Jing (Beihang University, Beijing, China) for his support in MPS technique. They would also like to acknowledge the instrumental and technical support of multimodal biomedical imaging experimental platform, Institute of Automation, Chinese Academy of Sciences, Beijing.

REFERENCES

[1] L. L. Israel, A. Galstyan, E. Holler, and J. Y. Ljubimova, "Magnetic iron oxide nanoparticles for imaging, targeting and treatment of primary and metastatic tumors of the brain," *J. Controlled Release*, vol. 320, pp. 45–62, Apr. 2020.

[2] Y. Du, X. Liu, Q. Liang, X.-J. Liang, and J. Tian, "Optimization and design of magnetic ferrite nanoparticles with uniform tumor distribution for highly sensitive MRI/MPI performance and improved magnetic hyperthermia therapy," *Nano Lett.*, vol. 19, no. 6, pp. 3618–3626, Jun. 2019.

[3] W. Tong et al., "Highly sensitive magnetic particle imaging of vulnerable atherosclerotic plaque with active myeloperoxidase-targeted nanoparticles," *Theranostics*, vol. 11, no. 2, pp. 506–521, 2021.

[4] L. Yin et al., "Recent developments of the reconstruction in magnetic particle imaging," *Vis. Comput. for Ind., Biomed., Art*, vol. 5, no. 1, p. 24, Oct. 2022.

[5] S. M. Dadfar et al., "Iron oxide nanoparticles: Diagnostic, therapeutic and theranostic applications," *Adv. Drug Del. Rev.*, vol. 138, pp. 302–325, Jan. 2019.

[6] Z. W. Tay et al., "Magnetic particle imaging-guided heating in vivo using gradient fields for arbitrary localization of magnetic hyperthermia therapy," *ACS Nano*, vol. 12, no. 4, pp. 3699–3713, Apr. 2018.

[7] Y. Liu et al., "Weighted sum of harmonic signals for direct imaging in magnetic particle imaging," *Phys. Med. Biol.*, vol. 68, no. 1, 2022, Art. no. 015018.

[8] G. Jia et al., "Gradient-based pulsed excitation and relaxation encoding in magnetic particle imaging," *IEEE Trans. Med. Imag.*, vol. 41, no. 12, pp. 3725–3733, Dec. 2022.

[9] S. E. Sandler, B. Fellows, and O. T. Mefford, "Best practices for characterization of magnetic nanoparticles for biomedical applications," *Anal. Chem.*, vol. 91, no. 22, pp. 14159–14169, 2019.

[10] J. Connolly and T. G. S. Pierre, "Proposed biosensors based on time-dependent properties of magnetic fluids," *J. Magn. Magn. Mater.*, vol. 225, nos. 1–2, pp. 156–160, Jan. 2001.

[11] B. Tian et al., "Attomolar Zika virus oligonucleotide detection based on loop-mediated isothermal amplification and AC susceptometry," *Biosensors Bioelectron.*, vol. 86, pp. 420–425, Dec. 2016.

[12] A. P. Astalan, F. Ahrentorp, C. Johansson, K. Larsson, and A. Krozer, "Biomolecular reactions studied using changes in Brownian rotation dynamics of magnetic particles," *Biosensors Bioelectron.*, vol. 19, no. 8, pp. 945–951, Mar. 2004.

[13] F. Ludwig et al., "Optimization of magnetic nanoparticles for magnetic particle imaging," *IEEE Trans. Magn.*, vol. 48, no. 11, pp. 3780–3783, Nov. 2012.

[14] S. Biederer et al., "Magnetization response spectroscopy of superparamagnetic nanoparticles for magnetic particle imaging," *J. Phys. D, Appl. Phys.*, vol. 42, no. 20, Oct. 2009, Art. no. 205007.

[15] M. Utkur and E. U. Saritas, "Simultaneous temperature and viscosity estimation capability via magnetic nanoparticle relaxation," *Med. Phys.*, vol. 49, no. 4, pp. 2590–2601, Apr. 2022.

[16] J. B. Weaver, A. M. Rauwerdink, and E. W. Hansen, "Magnetic nanoparticle temperature estimation," *Med. Phys.*, vol. 36, no. 5, pp. 1822–1829, May 2009.

[17] K. Wu, D. Su, R. Saha, J. Liu, V. K. Chugh, and J.-P. Wang, "Magnetic particle spectroscopy: A short review of applications using magnetic nanoparticles," *ACS Appl. Nano Mater.*, vol. 3, no. 6, pp. 4972–4989, Jun. 2020.

[18] K. Wu et al., "Magnetic nanoparticles and magnetic particle spectroscopy-based bioassays: A 15 year recap," *Nano Futures*, vol. 6, no. 2, Jun. 2022, Art. no. 022001.

[19] H. Khurshid, Y. Shi, B. L. Berwin, and J. B. Weaver, "Evaluating blood clot progression using magnetic particle spectroscopy," *Med. Phys.*, vol. 45, no. 7, pp. 3258–3263, Jul. 2018.

[20] N. Löwa, M. Seidel, P. Radon, and F. Wiekhorst, "Magnetic nanoparticles in different biological environments analyzed by magnetic particle spectroscopy," *J. Magn. Magn. Mater.*, vol. 427, pp. 133–138, Apr. 2017.

[21] X. Zhang et al., "Molecular sensing with magnetic nanoparticles using magnetic spectroscopy of nanoparticle Brownian motion," *Biosensors Bioelectron.*, vol. 50, pp. 441–446, Dec. 2013.

[22] F. Fidler et al., "Stem cell vitality assessment using magnetic particle spectroscopy," *IEEE Trans. Magn.*, vol. 51, no. 2, pp. 1–4, Feb. 2015.

[23] E. L. Rösch et al., "Point-of-need detection of pathogen-specific nucleic acid targets using magnetic particle spectroscopy," *Biosensors Bioelectron.*, vol. 192, Nov. 2021, Art. no. 113536.

[24] K. Wu et al., "One-step, wash-free, nanoparticle clustering-based magnetic particle spectroscopy bioassay method for detection of SARS-CoV-2 spike and nucleocapsid proteins in the liquid phase," *ACS Appl. Mate. Interfaces*, vol. 13, no. 37, pp. 44136–44146, Sep. 2021.

[25] J. Zhong, E. L. Rösch, T. Viereck, M. Schilling, and F. Ludwig, "Toward rapid and sensitive detection of SARS-CoV-2 with functionalized magnetic nanoparticles," *ACS Sensors*, vol. 6, no. 3, pp. 976–984, Mar. 2021.

[26] X. Cui, L. Li, and W. Liu, "A rapid and sensitive magnetic immunoassay of biomolecules based on magnetic nanoparticles," *IEEE Trans. Instrum. Meas.*, vol. 71, pp. 1–7, 2022.

[27] P. Vogel et al., "Critical offset magnetic particle spectroscopy for rapid and highly sensitive medical point-of-care diagnostics," *Nature Commun.*, vol. 13, no. 1, p. 7230, 2022.

[28] S. Draack et al., "Multiparametric magnetic particle spectroscopy of $CoFe_2O_4$ nanoparticles in viscous media," *J. Phys. Chem. C*, vol. 123, no. 11, pp. 6787–6801, Mar. 2019.

[29] T. Viereck, S. Draack, M. Schilling, and F. Ludwig, "Multi-spectral magnetic particle spectroscopy for the investigation of particle mixtures," *J. Magn. Magn. Mater.*, vol. 475, pp. 647–651, Apr. 2019.

[30] A. M. Rauwerdink, A. J. Giustini, and J. B. Weaver, "Simultaneous quantification of multiple magnetic nanoparticles," *Nanotechnology*, vol. 21, no. 45, Nov. 2010, Art. no. 455101.

[31] L. Tu, K. Wu, T. Klein, and J.-P. Wang, "Magnetic nanoparticles colourization by a mixing-frequency method," *J. Phys. D, Appl. Phys.*, vol. 47, no. 15, Apr. 2014, Art. no. 155001.

[32] P. Szwargulski et al., "Monitoring intracranial cerebral hemorrhage using multicontrast real-time magnetic particle imaging," *ACS Nano*, vol. 14, no. 10, pp. 13913–13923, Oct. 2020.

[33] C. Shasha, E. Teeman, K. M. Krishnan, P. Szwargulski, T. Knopp, and M. Möeddel, "Discriminating nanoparticle core size using multi-contrast MPI," *Phys. Med. Biol.*, vol. 64, no. 7, Apr. 2019, Art. no. 074001.

[34] S. Müessig, F. Fidler, D. Haddad, K.-H. Hiller, S. Wintzheimer, and K. Mandel, "Supraparticles with a magnetic fingerprint readable by magnetic particle spectroscopy: An alternative beyond optical tracers," *Adv. Mater. Technol.*, vol. 4, no. 9, Sep. 2019, Art. no. 1900300.

[35] Y. Sun, N. Ye, D. Wang, Z. Du, S. Bai, and T. Yoshida, "An improved method for estimating core size distributions of magnetic nanoparticles via magnetization harmonics," *Nanomaterials*, vol. 10, no. 9, p. 1623, Sep. 2020.

[36] S. Ota, K. Nishimoto, T. Yamada, and Y. Takemura, "Second harmonic response of magnetic nanoparticles under parallel static field and perpendicular oscillating field for magnetic particle imaging," *AIP Adv.*, vol. 10, no. 1, Jan. 2020, Art. no. 015007.

[37] D. B. Reeves and J. B. Weaver, "Magnetic nanoparticle sensing: Decoupling the magnetization from the excitation field," *J. Phys. D, Appl. Phys.*, vol. 47, no. 4, Jan. 2014, Art. no. 045002.